Chapter 4

A Distributed Population of Low Mass Pre-Main Sequence Stars near the Taurus Molecular Clouds[1]

In this chapter, I present a driftscan survey covering a $\sim 5^o \times 50^o$ region toward the Southern portion of the Taurus-Auriga molecular cloud. Data taken in the B, R, I filters (converted to g, r, i photometry) with the Quest-2 camera on the Palomar 48-inch telescope were combined with 2MASS near-infrared photometry to select candidate young stars. Follow-up optical spectroscopy of 190 candidates led to identification of 42 new low mass PMS stars with spectral types M4-M8, of which approximately half exhibit surface gravity signatures similar to known Taurus stars while the other half exhibit surface gravity signatures similar to members of the somewhat older Upper Sco, TW Hya and Beta Pic associations. The pre-main sequence stars are spread over $\sim 35^o$, and many are located well outside of previously explored regions. From assessment of the spatial and proper motion distributions, I argue that the new pre-main sequence stars identified far from the clouds cannot have originated from the vicinity of the 1–2 Myr-old subclusters which contain the bulk of the identified Taurus members, but instead represent a newly-identified area of recent star-formation near the clouds.

[1] A modified version of this chapter has been published previously as Slesnick, Carpenter, Hillenbrand, & Mamjek 2006, AJ, 132, 2665.

4.1 Motivation

The Taurus-Auriga molecular cloud complex has, for decades, been considered the quintessential example of low density, isolated star formation. This fact along with the proximity of Taurus (140 pc) and its position in the northern hemisphere has caused Taurus to be one of the most often studied star-forming regions. Several authors (e.g., Briceño et al. 1999, Luhman 2000, Briceño et al. 2002, Luhman et al. 2003a, Luhman 2004b, Guieu et al. 2006) have used optical/near-infrared/X-ray imaging to identify young star candidates within the clouds. Follow-up optical spectroscopy of photometrically selected candidates can distinguish members of Taurus from foreground or background field interlopers. These studies found the Taurus population is clustered into several loose aggregates (Gomez et al., 1993), and is predominantly very young ($\sim$1–2 Myr; e.g., Briceño et al. 1998, Hartmann 2000). Thus far, no conclusive evidence has been established for a widespread population of older stars within or near the cloud (Briceño et al., 1999).

The phenomenon of short timescale (1–2 Myr) clustered star-formation is not unique to Taurus but has been found in almost all other nearby young associations (e.g., Carpenter 2000, Palla & Stahler 2000). The large numbers of very young stars and apparent lack of more evolved (5–10 Myr-old) objects in star forming regions contrasts with ages of a few tens of megayears (e.g., Blitz & Shu 1980) inferred for molecular clouds. Either star-formation takes place for only a small fraction of the cloud lifetime, or molecular clouds themselves live only a few megayears (e.g., Hartmann et al. 2001).

An alternative explanation for the apparent lack of older stars in molecular clouds is that such objects have been missed in previous surveys. Limitations in telescope time and instrument fields of view have constrained most previous deep imaging surveys in Taurus (e.g., Briceño et al. 1999, Luhman 2000) to small areas focused on the subclusters (each $\sim$1 pc wide) known to contain most of the young members. Assuming a mean velocity dispersion of $\sim$2 km/s (Hartmann et al., 1986), a putative population of 5–10 Myr old stars in Taurus could travel up to $\sim$20 pc (8 deg) away

from its birth site.

Several studies (e.g., Neuhaeuser et al. 1997, Wichmann et al. 1996) have attempted to use the ROSAT All Sky Survey (RASS) with spectroscopic follow-up to identify G–mid K-type post T-Tauri Stars (stars with ages ∼3–10 Myr; PTTSs) far from the current Taurus members. These observations revealed a distributed population of lithium-rich stars (indicating that they are younger than ∼100 Myr) that are widely dispersed across the cloud and beyond. However, because both the decay of x-ray emission and the depletion of lithium occur slowly for G–type stars with ages <100 Myr, these data alone cannot discriminate whether the RASS-selected stars represent a 1 Myr-old or 10 Myr-old Taurus population, or a 100 Myr-old population that originated elsewhere. Consequently, the origin of these stars and their relation to Taurus is still controversial (e.g., Briceno et al. 1997). The largest optical/near-infrared imaging survey to date that searched for Taurus members is that of Luhman (2006) who used a combination of USNO and 2MASS magnitudes to find young brown dwarfs within a 15×15 deg^2 region centered on the known 1 Myr-old subclusters. The survey was aimed specifically at identifying young brown dwarfs with colors and magnitudes similar to known ∼1 Myr-old substellar Taurus members and was not targeted at finding older objects or comparably aged low mass stars. My survey includes regions beyond previously studied parts of the cloud, and is ideally suited to find slightly more evolved association members if they exist as counterparts to the young population.

4.2 Observations

I have used the Quest-2 camera to complete a new optical B, R, I (converted to g, r, i) imaging survey of ∼250 deg^2 near the Taurus molecular clouds. The specific survey area was chosen to include both well-known subclusters of stars (L 1536 and L 1529) and regions beyond previously studied parts of the cloud. Details of the photometric survey were given in chapter 2. My primary goal in Taurus is to search for and characterize a possible distributed population of pre-main sequence (PMS) stars

within and surrounding the clouds. In chapter 3, I combined the Taurus photometric data with 2MASS J, H, K_S photometry to select candidate young stars, and presented newly obtained spectral data for 190 of these candidates.

All spectral analysis was performed as outlined in chapter 3. Figure 4.1 shows measured indices for all PMS star spectral candidates observed in the Taurus region. In the left panel, two outliers (SCH J0429595+2433080 and SCH J0518028+2327126) sit below the primary sequence of data points. Both objects are confirmed to be young stars with strong Hα emission (indicating that the star is likely still accreting; see §5.3.3) and I attribute their position in the left panel of figure 4.1 to a small amount of veiling present in their spectra (see §3.2.3). In the right side of figure 4.1 measured indices for PMS candidates have been divided into three groups based on their surface gravity: circles represent objects with surface gravity lower (i.e., younger in age) than the Upper Sco association, triangles indicate objects with intermediate surface gravity comparable to the Upper Sco, TW Hya and Beta Pic associations, and black X's indicate field stars (see §4.3).

One difficulty in interpreting the right panel of figure 4.1 directly is that the Na-8190 index is contaminated by telluric features. The Taurus spectral data were taken at systematically lower airmasses than many of the spectral standards. As a result, a program star with intermediate gravity signatures observed at low airmass will have a lower Na-8190 index than an intermediate gravity standard of the same spectral type observed at high airmass. This effect causes a discrepancy between the positions of the green X's and the triangles in the right panel of figure 4.1.

Figure 4.2 shows a section of the spectra which highlights the Na I (8183 and 8195 Å) absorption feature for dwarf, intermediate, and low gravity stars of the same spectral type. Both GJ 866 and USco CTIO 53 (the dwarf and intermediate-gravity stars) were observed at high airmass whereas MHO 7 (the low gravity Taurus member) was observed at low airmass. Telluric absorption (8161–8282 Å) seen in the spectra of GJ 866 and USco CTIO 53 affects both the continuum band and Na I band causing systematically high measurements of the Na-8190 index. However, the three spectra can be clearly distinguished through visual inspection of the NaI line strengths. Thus,

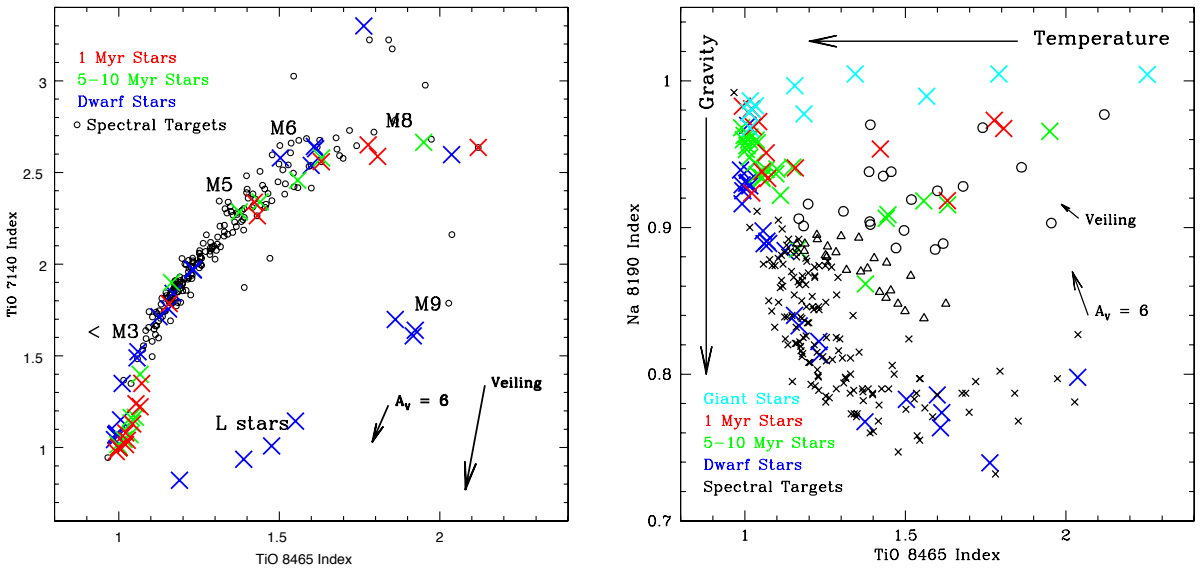

Figure 4.1 The left panel shows temperature-sensitive TiO-7140 vs. TiO-8465 indices; the right panel shows the TiO-8465 index vs. the gravity sensitive Na-8190 index. In both panels, blue X's represent measured indices for field dwarfs and members of the Hyades (∼650 Myr), Pleiades (∼115 Myr) and AB Dor (∼75–150 Myr) associations. Green X's show measured indices for intermediate-age spectral standards from Beta Pic (∼11 Myr), TW Hya (∼8 Myr), and Upper Sco (∼5 Myr). Red X's show measured indices for young Taurus members (∼1–2 Myr). Cyan X's which in the right panel represent measured indices for giant standard stars. In both panels, the effects of extinction and veiling are shown as vectors (see §3.2.3). Black symbols are measured indices for Taurus PMS candidates. In the right panel, these symbols are divided into three groups based on inferred surface gravity: circles represent objects with surface gravity lower (i.e., younger in age) than the Upper Sco association, triangles indicate objects with intermediate surface gravity comparable to the Upper Sco, TW Hya and Beta Pic associations, and black X's indicate field stars.

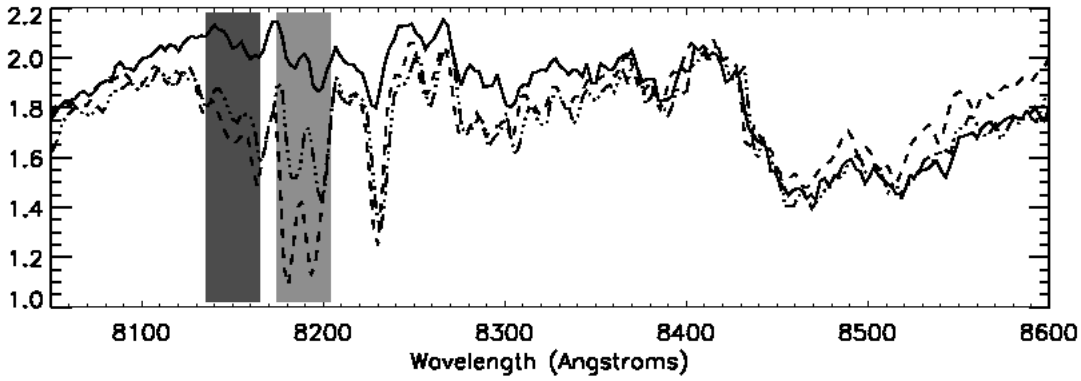

Figure 4.2 Section of the optical spectrum highlighting the surface gravity sensitive Na I doublet (8183 and 8195 Å). The dashed spectrum is an M5V star (GJ 866; Kirkpatrick et al. 1991), the dotted-dashed spectrum is an M5 Upper Sco member (USco CTIO 53; Ardila et al. 2000), and the solid spectrum is an M5 Taurus member (MHO 7; Briceño et al. 1998). Light and dark shaded regions show the respective locations of the Na I and the continuum bands used in constructing the Na-8190 index. All spectra have been normalized at 8410 Å near the temperature-sensitive TiO (8465 Å) molecular absorption band. Both GJ 866 and USco CTIO 53 were observed at high airmass and telluric absorption (8161-8282 Å) affects both the continuum band and Na I band, causing systematically high measurements of the Na-8190 index. However, gravity signatures in the three spectra can be distinguished clearly through visual inspection of the line strengths.

I used the quantitative indices as a rough guide only, and all final gravity classification was done by eye.

Table 4.1. Measured quantities for new PMS stars near Taurus

ID[a]	g	r	i	J[c]	H[c]	K_S[c]	TiO-7140	TiO-8165	Na-8195	SpType[d]	$W(H\alpha)$ [Å]	Age[e]
SCH J0325332+2426581	18.0	16.4	14.7	12.34	11.72	11.47	2.02	1.30	0.89	M4.5	-10	int
SCH J0359099+2009362	19.8	18.0	16.1	13.47	12.89	12.53	2.32	1.42	0.85	M4.75	-7	int
SCH J0400220+2232382	–	18.4	16.3	13.45	12.76	12.45	2.23	1.36	0.87	M4.75	-6	int
SCH J0400279+2031593	20.0	18.2	16.1	13.14	12.56	12.23	2.54	1.49	0.84	M5.75	-16	int
SCH J0407246+2332554	18.4	16.7	14.8	12.77	12.06	11.85	1.69	1.16	0.88	M4	-6	int
SCH J0407350+2237396	18.6	16.8	15.0	12.16	11.60	11.25	2.38	1.51	0.86	M5	-16	int
SCH J0412433+2055306	–	20.3	17.8	14.24	13.53	13.17	2.97	1.95	0.90	M8	-15	int
SCH J0416272+2053093[b]	18.6	16.8	14.9	12.05	11.47	11.11	2.26	1.43	0.93	M5	-5	young
SCH J0420068+2432267	17.5	16.1	14.6	12.42	11.87	11.59	1.84	1.18	0.88	M4	–	int
SCH J0420491+2327370	18.3	16.7	14.9	12.07	11.39	11.09	2.03	1.25	0.88	M4.25	-8	int
SCH J0426452+2131408	19.3	17.8	15.8	13.19	12.64	12.31	2.23	1.38	0.87	M4.75	-8	int
SCH J0427074+2215039	–	17.7	15.4	12.27	11.64	11.29	2.64	1.74	0.96	M6.75	-18	young
SCH J0429595+2433080[b]	–	17.9	15.7	11.68	10.53	9.81	1.87	1.39	0.97	M5.5	-71	young
SCH J0431191+2335048[b]	–	20.3	17.5	13.50	12.71	12.19	2.63	2.12	0.97	M8	-32	young
SCH J0433131+2025200	–	19.1	17.0	14.20	13.46	13.14	2.36	1.40	0.87	M5	-12	int
SCH J0434454+2308035	20.2	18.2	16.0	12.80	12.02	11.70	2.31	1.45	0.93	M5.25	-11	young
SCH J0438001+2327167	19.7	18.0	15.9	13.27	12.66	12.34	2.41	1.45	0.85	M5.25	-15	int
SCH J0438163+2326404	17.7	16.2	14.3	11.80	11.24	10.96	2.24	1.38	0.93	M4.75	-7	young
SCH J0438586+2336352	18.4	16.8	14.3	11.97	11.36	11.03	2.03	1.19	0.91	M4.25	-15	young
SCH J0438587+2323596	19.1	17.5	15.3	12.49	11.93	11.59	2.62	1.68	0.92	M6.5	-14	young
SCH J0439016+2336030	16.7	15.2	12.8	11.33	10.59	10.18	2.41	1.60	0.92	M6	-62	young
SCH J0439064+2334179	19.0	17.3	14.6	12.09	11.53	11.19	2.78	1.86	0.94	M7.5	-8	young
SCH J0439410+2304262	–	19.1	17.1	14.41	13.81	13.46	2.09	1.31	0.87	M4.5	-12	int
SCH J0439507+2133564	–	19.7	17.5	14.43	13.80	13.43	2.67	1.62	0.84	M6	-8	int

Table 4.1 (cont'd)

ID[a]	g	r	i	J[c]	H[c]	K_S[c]	TiO-7140	TiO-8165	Na-8195	SpType[d]	$W(H\alpha)$ [Å]	Age[e]
SCH J0440534+2055473	18.8	17.1	15.1	12.48	11.88	11.62	2.32	1.44	0.87	M5.	-11	int
SCH J0502377+2154050	19.2	17.4	15.6	13.16	12.53	12.20	1.99	1.25	0.88	M4.25	-10	int
SCH J0506466+2104298	18.1	16.5	14.6	12.05	11.40	11.11	2.43	1.51	0.91	M5.25	-14	young
SCH J0516021+2214530	17.4	15.9	14.1	11.67	11.13	10.75	2.25	1.39	0.90	M5	-10	young
SCH J0516058+2236152	19.1	17.2	15.6	13.29	12.59	12.30	1.88	1.18	0.88	M4	-8	int
SCH J0518028+2327126	18.6	17.2	15.3	12.99	12.32	11.88	2.03	1.47	0.88	M5	-21	young
SCH J0522333+2439254	18.9	17.0	15.2	12.75	12.04	11.72	2.18	1.38	0.90	M4.75	-7	young
SCH J0522335+2439197	19.2	17.2	15.3	12.79	12.14	11.79	2.10	1.30	0.91	M4.5	-8	young
SCH J0523020+2428087	18.1	16.4	14.8	12.60	11.92	11.61	1.78	1.16	0.90	M4	-3	int
SCH J0523500+2435237	–	18.7	16.6	13.81	13.14	12.77	2.63	1.61	0.88	M6	-18	young
SCH J0531021+2333579	17.5	16.0	14.0	12.28	11.64	11.39	1.79	1.18	0.90	M4	-5	int
SCH J0531026+2334022	17.6	16.0	13.9	12.26	11.58	11.35	1.83	1.22	0.89	M4	-5	int
SCH J0532021+2423030	19.9	18.2	16.2	13.69	13.06	12.80	2.50	1.44	0.85	M5	-19	int
SCH J0533363+2102276	17.4	15.8	14.2	11.93	11.32	11.07	2.05	1.28	0.88	M4.5	-7	int
SCH J0534480+2243142	18.2	16.6	15.0	12.83	12.18	11.93	1.94	1.22	0.89	M4.25	-6	young
SCH J0536190+2242428	17.7	16.3	14.5	12.13	11.53	11.27	2.17	1.35	0.89	M4.75	-12	int
SCH J0537385+2428518	17.8	16.2	14.2	11.66	11.06	10.78	2.44	1.49	0.89	M5.25	-14	young
SCH J0539009+2322081	19.1	17.6	15.3	12.68	12.10	11.79	2.53	1.59	0.88	M6	-16	young

[a]Object IDs given in J2000 coordinates.

[b]Three of the PMS objects discussed in this work were previously identified in the literature: SCH J0429595+2433080 (Guieu et al. 2006), SCH J0431191+2335048 (Luhman 2006), and SCH J0416272+2053093 (Wichmann et al. 1996)

[c]Near-infrared photometry taken from 2MASS.

[d]Spectral type uncertainties are ±0.5 subclasses.

[e]An age of 'int' indicates the star exhibited surface gravity-sensitive spectral features consistent with those of 5–10 Myr-old stars. Stars labeled 'young' have gravity signatures that indicate the star is only 1 to a few Myr-old.

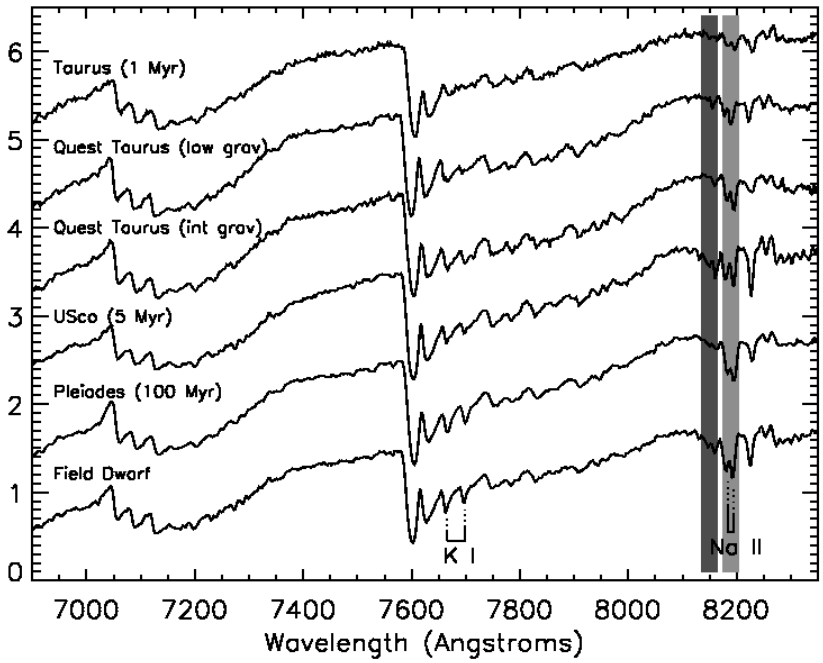

Figure 4.3 Spectra of M4/M4.5 stars presented in order of decreasing surface gravity (bottom to top). Spectra shown are of a field dwarf, a 115 Myr Pleiades object, a 5 Myr Upper Sco member, a new Quest-2 Taurus candidate identified to have Upper Sco-type intermediate gravity, a new Quest-2 Taurus candidate identified to have low gravity, and a 1 Myr Taurus star. Surface gravity sensitive features include the K I doublet (7677 Å) and the Na I doublet (8189 Å).

4.3 Discussion

For the remainder of this analysis, objects with surface gravity features weaker than those of the intermediate-age standards are considered by me to have low gravity; objects with gravity features similar to those exhibited by the intermediate-age standards are considered to have intermediate gravity. Based on this classification scheme I identify 42 new PMS stars (see table 4.1). Within the 42 new PMS stars, I identify 19 objects to have spectral features which indicate lower surface gravity than members of Upper Sco (∼5 Myr). Most of the new low gravity objects have inferred gravities as low as those similarly inferred for known 1–2 Myr Taurus members. Of these 19 objects, three were previously identified in the literature: SCH J04295950+2433080 (Guieu et al., 2006), SCH J04311908+2335048 (Luhman, 2006)

and SCH J0416272+2053093 (Wichmann et al., 1996). I additionally identify 23 objects that have intermediate-strength surface gravity features consistent with those observed in Upper Sco, TW Hya and Beta Pic stars. In figure 4.3 I present spectra of M4/M4.5 stars shown in order of decreasing surface gravity and decreasing Na I and K I absorption (bottom to top). All spectra of observed stars as old as AB Dor or the Pleiades (∼100 Myr) appear identical to those of dwarf stars. Therefore, the intermediate-age population in Taurus is likely significantly younger than ∼100 Myr, although the exact upper bound on the age of this population is unknown due to lack of comparison stars with ages between 10 and 100 Myrs. This interpretation may also apply to three objects identified by Luhman (2006) which were found to have gravity intermediate between Taurus and dwarf stars and presumed in that study to be ∼100 Myr-old due to lack of comparison stars with ages between those of Taurus members and field dwarfs. Hereafter I refer to the low gravity objects as "young" and the intermediate gravity objects as "intermediate-age." In the color-magnitude and color-color diagrams (figure 3.3 and figure 3.4), candidates for which I have obtained spectral data are shown as large symbols. Photometric and spectral data for new PMS stars are given in table 4.1. Table 4.2 contains magnitudes and spectral index measurements for PMS candidates spectroscopically determined to be field dwarfs.

Understanding the relationship of the newly-identified PMS population to the known Taurus members requires distances to the new PMS stars which I can not determine based on the current data set. If I assume they are located at the distance of Taurus, the derived ages from an HR diagram are ∼1–10 Myr, and the intermediate-age stars tend to have systematically lower derived luminosities than the young stars at a given spectral type. While these relative ages are consistent with those derived from surface gravity analysis, a range of distances could yield similar luminosity segregation results. In lieu of distance measurements, I constrain the origin of the PMS objects identified in this work by assessing the projected spatial distribution and kinematics of the new young and intermediate-age stars in relation to the known Taurus population.

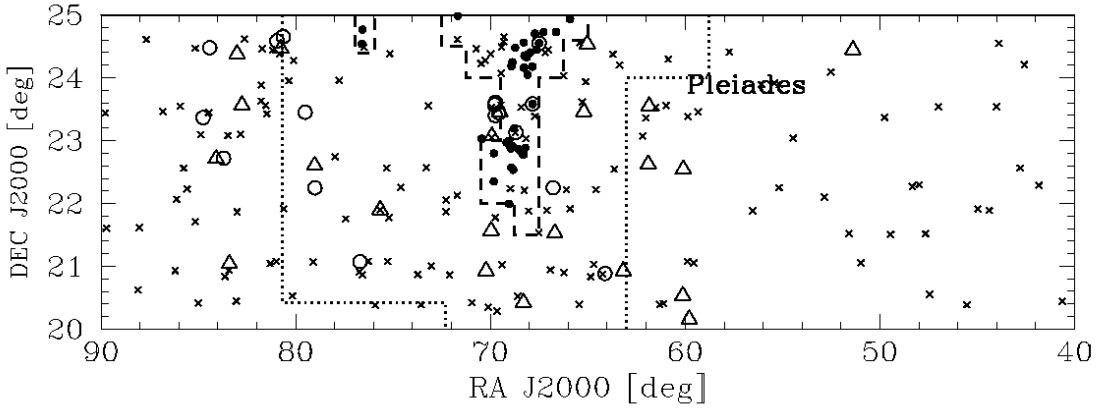

Figure 4.4 Spatial area of the imaging survey shown with previously known low mass Taurus members (filled circles; see text for references). Dashed lines indicate the boundary of previous deep CCD imaging surveys aimed at identifying new 1 Myr-old association members. Dotted lines indicate the boundary a 5 Myr old star with velocity 2 km/s could have traveled from any of the known subclusters. Open circles and triangles represent new low and intermediate-gravity stars identified from this work. Black X's show spectral candidates determined to be field dwarfs. The location of the Pleiades cluster (α=57 deg, δ=24 deg) is indicated.

4.3.1 Spatial Distribution of New PMS Stars

The new young and intermediate-age stars are distributed throughout the survey region, and many are located well beyond regions previously explored for young PMS stars. Figure 4.4 shows the location of spectroscopically observed Quest-2 candidates, along with known low mass Taurus members from the literature (Briceño et al. 2002, Guieu et al. 2006, Hartmann 2002, Luhman et al. 2003a, Luhman 2004b, Luhman 2006). The region that has been previously studied for low mass stars using deep optical/near-infrared imaging with spectroscopic follow-up (Briceño et al. 2002, Guieu et al. 2006, Luhman 2000, Luhman et al. 2003a, Luhman 2004b) is indicated, as is the Pleiades association. Based on comparison with CO maps of the region (Dame et al., 2001), while some objects do lie in projection near molecular gas, I see no systematic correlation between the spatial distribution of the new PMS stars and the CO emission.

To assess whether the new PMS stars are associated with the known concentrations of Taurus members or whether they are more uniformly distributed, I show in

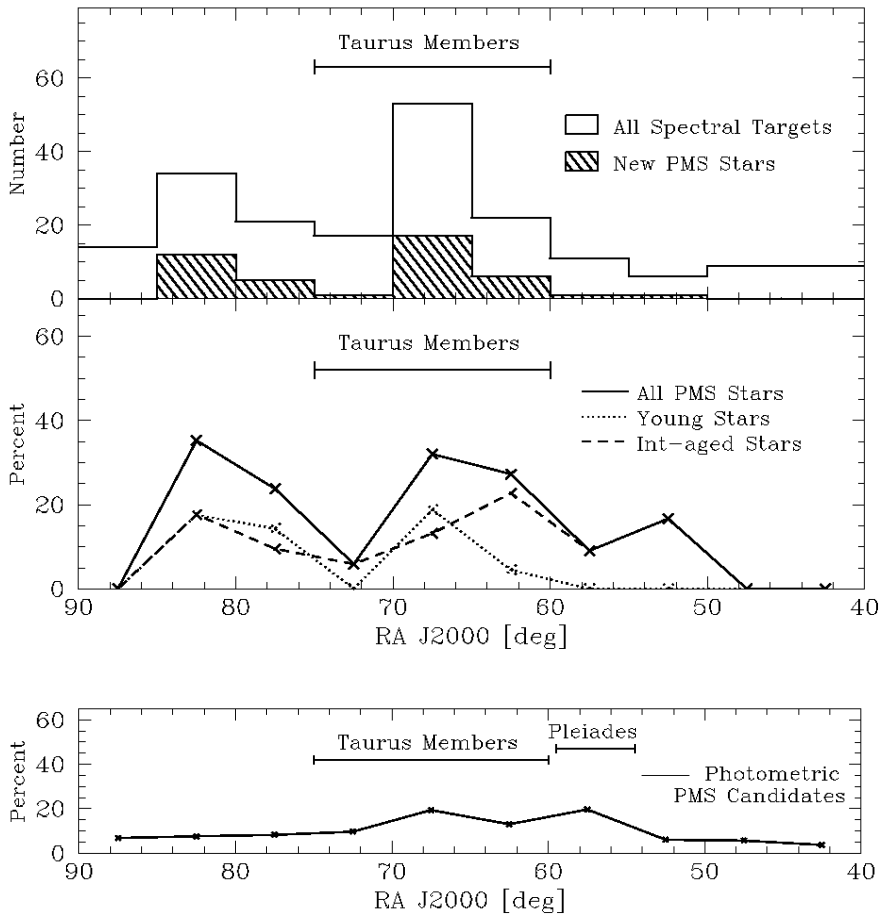

Figure 4.5 Top panel shows, as a function of RA, histograms for the total number of stars observed spectroscopically (open histogram) and those that were determined to be PMS stars (hatched histogram). Middle panel indicates the percentage of spectroscopically observed objects classified as PMS stars (solid line), and separately the percentage determined to be young (dotted line) or intermediate-age (dashed line) stars based on spectroscopic signatures of surface gravity. The RA range containing 98% of known low mass Taurus members is shown. Bottom panel shows the percentage of the ∼1800 photometric PMS candidates which fall at a given RA.

figure 4.5 a histogram of the RA values for all sources with spectra presented here and for those sources confirmed as PMS objects. In the middle panel I present the percentage of spectroscopically observed objects determined to be PMS stars. These can be compared to the RA range that contains 98% of the known low mass Taurus members (Briceño et al. 2002, Guieu et al. 2006, Hartmann 2002, Luhman et al. 2003a, Luhman 2004b, Luhman 2006). The bottom panel shows the percentage of the 1800 photometric candidates (see §3.1) located within a given RA range.

I note two spatial concentrations of new PMS stars: one near the known Taurus members at $\alpha \approx 68^o$, and a second in the eastern portion of the cloud centered around $\alpha \approx 82^o$. In figure 4.4 I indicate the approximate boundary within which a 5 Myr star with velocity 2 km/s relative to Taurus could have traveled from any of the known Taurus subclusters. Some of the young objects newly identified here are located well beyond this region. Assuming an age of <5 Myr as derived from surface gravity analysis, if these new young stars originated in the known star-forming subclusters they must, therefore, have arrived at their current positions at relatively high velocities.

An alternative, and perhaps more likely scenario is that I have identified a previously unknown area of recent star-formation outside of the current dense cloud complex. To further quantify the new PMS population and assess this possibility, I divide my PMS stars into 3 groups: those that lie in the same RA range as 98% of the known Taurus sample ($60^o \leq \alpha \leq 75^o$), those that are east ($\alpha > 75^o$) and those that are west ($\alpha < 60^o$) of this RA range. I find that of the 190 spectral candidates, 2/33 (6%) are confirmed to be PMS stars in the western region, 23/89 (26%) in the central region, and 17/68 (25%) in the eastern region. Spectroscopic confirmation rates of 25% in the east and only 6% in the west are contrary to the isotropic distribution I would expect to observe if these stars had been dispersed from the central regions. Using the two-tailed Fisher Exact test I compute a probability of ∼3% that the observed eastern and western distributions could have been drawn from the same population. I can therefore conclude with 97% confidence that the distributed PMS stars were not randomly dispersed from the known 1–2 Myr-old Taurus population. Instead, I suggest that they likely represent a population that is not associated with

the currently visible areas of the dense Taurus-Auriga molecular cloud complex.

4.3.2 Proper Motion Analysis

A primary goal of my large-area survey is to search for and characterize any PMS stars that might exist far from the ∼1–2 Myr-old subclusters in Taurus. Having identified several tens of such stars, I can use proper motion information to further study the characteristics of this spectroscopically selected sample.

I extracted USNO-B1.0 proper motions[2] (Monet et al., 2003) for 141 of the 190 objects with spectra. Figure 4.6 shows histograms of the α and δ proper motion components for new young and intermediate-age PMS targets and for stars classified as field dwarfs. Because proper motions listed in the USNO catalog are relative rather than absolute (i.e., the proper motions of background stars have not been accounted for), it was necessary to extract similarly derived USNO proper motions of known Taurus members for comparison rather than using more accurate values listed in the literature (e.g., Frink et al. 1997). The bottom panels of figure 4.6 show histograms of USNO proper motions for 160 previously known Taurus members and for 58 Hipparcos-selected Pleiades members (Robichon et al., 1999).

The proper motions of the PMS stars appear strongly correlated (independent of RA) and distinct from the proper motions of Pleiades members, whereas the spectroscopic field dwarfs exhibit a very broad distribution of proper motions. These results indicate that the newly identified PMS population is not associated with the Pleiades and is not a collection of random field stars. Further, the PMS stars farthest from the known Taurus population do not exhibit systematically higher proper motions, as would have been expected if they had been ejected from the current star-forming regions, giving further evidence that I have identified a new region of relatively recent

[2]I define an object to have a measured USNO proper motion if it has either a non-zero proper motion or a non-zero proper motion uncertainty in the USNO-B1.0 Whole Sky catalog (Monet et al., 2003). This cut biases my analysis against objects with intrinsically small (proper motion <2 mas/yr) but well-measured (uncertainty < 2 mas/yr) proper motions which will be listed with μRA=0, μDec=0, μRA_err=0 and μDec_err=0. However, because the USNO proper motion measurements are rounded to the nearest mas/yr and non-measurements are not indicated, I am unsure when a measured proper motion uncertainty of zero refers to a very small uncertainty vs. a non-detection. Therefore, I feel this is a necessary, if conservative, selection criteria.

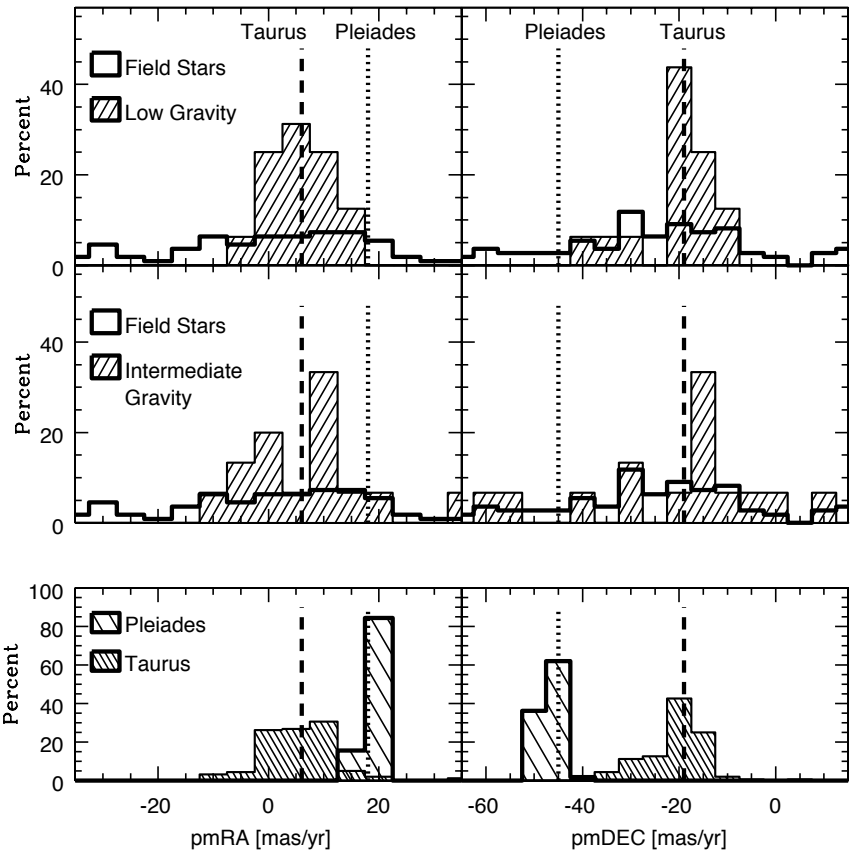

Figure 4.6 Histograms of proper motions extracted from the USNO-B1.0 catalog. In the top and middle panels, open histograms represent proper motions for stars which were spectroscopically determined to be field dwarfs; hatched histograms represent proper motions for new young (top) and intermediate-age (middle) PMS targets. In the bottom panels the light hatched histogram shows USNO-B1.0 proper motions for a sample of Pleiades members; the dark hatched histogram shows equivalent data for the sample of known Taurus members indicated in figure 4.4. All histograms have been normalized for ease of comparison and average values for Taurus and the Pleiades are shown in all panels. Data have been binned by 5 mas/yr. The average measured uncertainty for new PMS candidates is 4 mas/yr.

star-formation within the eastern regions of the clouds. The young sample in particular appears to have proper motions consistent with Taurus. A possible interpretation of these data is that the new PMS objects in the central regions are associated with the known Taurus population and the new PMS objects farther away were formed out of molecular material sharing a similar velocity and distance to that forming the current 1 Myr-old population. However, typical USNO proper motion uncertainties are large ($\pm$4 mas/yr), and the Taurus data themselves exhibit a large spread (bottom panels of figure 4.6). Therefore, a more detailed kinematic study of these objects is necessary before a definitive conclusion about their origin can be drawn (§4.5).

4.4 A New Distributed Population and the PTTS Problem

There has been much debate over the last few decades as to whether there exists a population of 3–10 Myr old post T-Tauri stars associated with the current 1–2 Myr old Taurus members. Spectroscopic follow-up studies of RASS-selected sources have identified a widespread population of stars in the vicinity of Taurus (e.g., Neuhaeuser et al. 1997, Wichmann et al. 1996), but the distances, ages, and origins of these stars remain controversial. Measures of x-ray emission and lithium equivalent widths are consistent with any ages from $\sim$1 to 100 Myr for these objects, and the nearly uniform spatial distribution of this population is consistent with its originating from a number of sources other than Taurus (e.g., Briceno et al. 1997). I have compared the spatial location of the new PMS sources identified here to the distribution of RASS sources in the area (e.g., Guillout et al. 1998) and find no correlation between areas of dense x-ray sources detected in the RASS and the newly identified stars in the eastern part of my survey region.

Besides X-ray emission, an efficient method of identifying nearby older PMS stars over a large area is through optical and near-infrared imaging combined with spectroscopic follow-up observations. Surface gravity signatures present in optical spec-

tra of late-K and M stars offer the advantage of clearly distinguishing young and intermediate-age PMS stars from 75–100 Myr-old stars. Considering the large number of imaging/spectroscopic surveys in the Taurus region, a natural question to ask is, how were the PMS stars presented here not discovered prior to my survey?

The primary reason these objects were not identified in earlier work is that I have searched much farther away from the clouds than most previous photometric/spectroscopic studies. The large-area work by Luhman (2006) probed only as far east as $\alpha \approx$5 hr and did not extend to the large number of newly discovered PMS stars in the eastern portion of my survey at $\alpha >$80 deg. Additionally, my survey occupies a unique range in color/magnitude space. Low mass stars discovered in early CCD surveys (e.g., Briceño et al. 2002) are saturated in the Quest-2 data. More recent surveys (e.g., Luhman 2004b, Guieu et al. 2006, Luhman 2006) have been concerned primarily with finding new brown dwarfs with spectral types $\geq$M6, which will be predominantly fainter and redder than the candidates discussed here. Indeed, comparison of USNO-$I2$ and 2MASS-J, H, K_S photometry for the Quest-2 PMS candidates to those selected in the Luhman (2006) study reveals that the Quest-2 candidates are systematically bluer. Despite the large overlap in area ($\sim$50 deg^2), the only observed candidate in my survey with spectral type $\geq$M6 selected as a candidate via the Luhman (2006) criteria is the one star (SCH J04311908+2335048) which our two works both identified. It is unlikely that the intermediate-age objects found in this work, which are predominantly bluer than the young objects (see figure 3.3), would have been selected as candidate Taurus members in any of the previous optical studies.

While I have discovered a new distributed population of both young and intermediate-age stars, I do not at this time claim that these objects represent the 'missing' post T-Tauri stars in Taurus. The spatial distribution of the PMS stars identified far from the known members is not consistent with those stars being associated with the Taurus subclusters. Additionally, the fact that the proper motions for the new young stars located tens of degrees away are consistent with known Taurus members implies that they were not ejected at high velocities from the current star-forming regions. Because my dataset is not complete either spatially or in magnitude/color

space (due to difficulties with weather and calibration), I cannot assess the full extent of this new population. Rather, I note that its existence hints there may be many more as-yet undiscovered PMS objects waiting to be identified in and surrounding the Taurus clouds.

4.5 Future Work

Radial velocities from high resolution spectra for all 42 new PMS stars combined with more robust proper motion measurements derived from existing catalogs will allow me to compute a 3D U, V, W velocity for each object over a range of distances. In addition, lithium equivalent widths can help confirm the youth of the new PMS sample which is currently based on NaI and KI line strengths. While lithium depletion occurs slowly over >100 Myr for G type stars and is therefore not suitable for distinguishing PTTSs from 100 Myr objects at these temperatures, for K to mid-M type stars that are fully convective, lithium depletion occurs over much faster timescales ($\sim$10 Myr; e.g., D'Antona & Mazzitelli 1994), and is a more robust indicator of youth. Finally, I emphasize that the new PMS population of 42 stars and a spectroscopic confirmation rate of $\sim$20% implies that several hundred similar young and intermediate-age PMS stars may be present in my larger photometric database.

Table 4.2. Measured quantities for candidates spectroscopically confirmed as field dwarfs near Taurus

ID[a]	g	r	i	J[c]	H[c]	K_S[c]	TiO-7140	TiO-8165	Na-8195
SCH J02423426+20262686[b]	17.3	–	14.4	12.53	11.98	11.69	1.55	1.07	0.87
SCH J02471836+22171512	–	20.2	17.9	14.58	13.94	13.49	3.17	1.85	0.76
SCH J02502040+24124969	18.4	16.5	14.9	12.55	11.94	11.63	1.98	1.22	0.81
SCH J02511084+22335835	17.8	16.1	14.7	12.52	11.90	11.66	1.84	1.16	0.86
SCH J02553616+24324815	19.2	17.3	15.5	12.82	12.18	11.83	2.28	1.35	0.77
SCH J02560113+23322159	19.2	17.5	15.4	13.13	12.55	12.21	2.11	1.26	0.78
SCH J02573373+21531119	17.0	15.4	13.9	11.58	11.03	10.74	1.84	1.14	0.84
SCH J02595189+21544806	18.8	17.1	15.5	13.00	12.36	12.07	2.03	1.25	0.82
SCH J03020861+20231122	17.3	15.7	14.0	11.68	11.05	10.79	2.06	1.25	0.88
SCH J03075903+23322049	17.6	16.0	14.0	12.31	11.74	11.46	1.71	1.10	0.84
SCH J03094953+20331863[b]	–	–	17.2	14.33	13.80	13.40	2.51	1.51	0.82
SCH J03103858+21311454	–	19.3	17.1	14.17	13.59	13.23	2.49	1.54	0.79
SCH J03115647+22180844	17.4	15.9	14.1	11.63	11.06	10.74	2.00	1.24	0.81
SCH J03132170+22162027	–	17.8	15.9	13.39	12.85	12.50	2.26	1.35	0.81
SCH J03174808+21303385	–	19.6	17.1	13.82	13.20	12.83	3.22	1.84	0.78
SCH J03190120+23221434	17.7	16.1	14.5	12.40	11.79	11.49	1.89	1.18	0.81
SCH J03235205+21031471	–	19.3	17.2	14.38	13.81	13.37	2.60	1.53	0.78
SCH J03262127+21311647	19.9	18.2	16.5	14.22	13.61	13.36	2.03	1.25	0.80
SCH J03300514+24052826	19.3	17.3	15.3	12.38	11.75	11.38	2.53	1.59	0.78
SCH J03312473+22060010	17.7	16.0	14.3	11.86	11.28	10.98	2.07	1.28	0.82
SCH J03374928+23022559	19.3	17.4	15.7	13.33	12.79	12.52	2.16	1.27	0.81
SCH J03403619+23533219	–	16.6	15.0	12.77	12.15	11.87	1.91	1.19	0.84
SCH J03404340+22150722	16.4	17.9	15.9	13.14	12.56	12.18	2.66	1.53	0.75
SCH J03414241+23545753	–	19.8	17.7	14.68	14.09	13.73	2.45	1.47	0.82
SCH J03441969+23534558	–	19.3	17.2	14.34	13.65	13.30	2.09	1.29	0.82
SCH J03461023+21525651	–	19.8	17.7	14.62	13.93	13.56	2.72	1.79	0.80
SCH J03505739+24244507	20.0	18.3	16.6	14.06	13.49	13.12	2.34	1.31	0.79
SCH J03571934+23273777	19.5	18.0	16.4	13.98	13.40	13.08	1.85	1.21	0.85
SCH J03581419+21030390	18.8	17.0	15.1	12.24	11.66	11.33	2.20	1.36	0.79
SCH J03592666+23230761	17.1	15.6	13.8	11.51	10.91	10.65	1.89	1.19	0.80
SCH J03593125+21044985	–	20.8	18.2	14.47	13.75	13.38	2.68	1.97	0.79
SCH J04032860+24175096	19.4	17.4	15.4	12.65	12.09	11.75	2.33	1.34	0.77
SCH J04032860+24175096	19.4	17.4	15.4	12.65	12.09	11.75	2.32	1.45	0.80
SCH J04035482+23334369	–	18.8	16.8	14.20	13.59	13.26	2.31	1.34	0.77
SCH J04042706+20243026	16.8	15.2	13.5	11.21	10.59	10.32	1.90	1.19	0.82
SCH J04051322+20233680	18.8	17.0	15.4	12.99	12.41	12.12	1.98	1.25	0.87
SCH J04055922+23314683	20.3	18.4	16.4	14.03	13.34	13.03	1.98	1.23	0.78

Table 4.2 (cont'd)

ID[a]	g	r	i	J[c]	H[c]	K_S[c]	TiO-7140	TiO-8165	Na-8195
SCH J04080508+23213945	18.1	17.4	15.7	13.25	12.68	12.35	2.28	1.36	0.78
SCH J04084314+23042360	–	19.5	17.1	14.03	13.57	13.20	3.02	1.54	0.75
SCH J04132997+24121104	19.7	17.8	15.9	13.64	12.90	12.61	1.63	1.08	0.84
SCH J04143471+22324170	18.0	16.2	14.7	12.36	11.77	11.47	1.82	1.14	0.79
SCH J04145027+24223723	18.4	16.7	15.0	12.47	11.90	11.59	1.93	1.22	0.79
SCH J04165655+20523604	–	19.3	17.0	13.66	13.03	12.60	2.59	1.68	0.78
SCH J04181857+22132340	17.7	15.8	14.0	11.17	10.54	10.20	2.38	1.41	0.77
SCH J04184558+21015469	20.1	18.2	16.2	13.14	12.53	12.21	2.43	1.44	0.79
SCH J04192264+20500801	18.4	16.7	15.3	13.13	12.45	12.16	1.57	1.10	0.87
SCH J04202448+23561330	–	20.6	18.4	14.60	13.85	13.42	2.16	2.03	0.82
SCH J04210820+23370654	19.9	18.6	16.6	13.89	13.31	12.97	2.48	1.39	0.78
SCH J04213745+24333974	–	19.1	17.1	14.35	13.72	13.39	2.40	1.40	0.76
SCH J04214590+20234439	–	19.7	17.2	13.94	13.34	12.92	2.72	1.71	0.79
SCH J04233635+21545582	18.4	17.0	15.3	12.99	12.35	12.11	1.88	1.17	0.81
SCH J04242298+22130276	18.5	17.0	15.2	12.70	12.06	11.74	1.79	1.16	0.88
SCH J04245196+20540815	19.2	17.7	15.9	13.44	12.80	12.55	1.81	1.15	0.85
SCH J04245748+24020200	–	19.4	16.7	13.37	12.73	12.35	3.22	1.78	0.73
SCH J04273712+20563907	20.0	18.2	16.0	13.08	12.45	12.07	2.54	1.52	0.78
SCH J04280637+24265280	19.8	17.6	15.8	12.97	12.00	11.58	1.34	1.03	0.91
SCH J04281979+21532986	18.5	16.9	15.2	12.86	12.29	12.02	2.00	1.20	0.79
SCH J04284465+24241965	20.3	18.4	16.2	13.35	12.73	12.33	2.64	1.50	0.77
SCH J04300382+21320646	20.2	18.5	16.6	14.06	13.45	13.13	2.27	1.33	0.84
SCH J04304952+23231579	–	20.2	18.1	15.27	14.69	14.12	1.78	1.16	0.88
SCH J04320885+21525117	17.8	16.3	14.7	12.54	11.89	11.67	1.85	1.17	0.82
SCH J04324101+23020399	20.1	18.2	16.6	13.45	12.31	11.75	0.94	0.96	0.99
SCH J04330156+22123664	–	18.8	16.9	14.21	13.44	13.08	1.93	1.19	0.86
SCH J04333877+23320263	–	18.6	16.4	13.86	13.09	12.76	1.84	1.16	0.88
SCH J04342548+20313479	18.6	16.8	15.1	12.73	12.08	11.83	1.95	1.21	0.87
SCH J04345291+23073158	19.6	17.6	15.8	13.31	12.51	12.20	1.66	1.11	0.86
SCH J04345328+23073237	–	19.1	17.1	14.66	13.98	13.60	1.76	1.26	0.82
SCH J04345328+23073237	–	19.1	17.1	14.66	13.98	13.60	1.80	1.17	0.83
SCH J04345328+23073237	–	19.1	17.1	14.66	13.98	13.60	1.81	1.16	0.83
SCH J04355509+22142525	–	18.3	16.5	14.03	13.36	13.07	1.99	1.25	0.87
SCH J04371222+24390300	–	18.6	16.7	14.05	13.54	13.07	2.29	1.38	0.79
SCH J04371755+24343438	17.8	16.1	14.6	12.50	11.83	11.59	1.73	1.11	0.89
SCH J04373727+21013612	17.1	15.6	14.1	12.07	11.46	11.21	1.81	1.15	0.86
SCH J04374450+24292963	–	19.7	17.4	14.46	13.83	13.39	2.67	1.56	0.77

Table 4.2 (cont'd)

ID[a]	g	r	i	J[c]	H[c]	K_S[c]	TiO-7140	TiO-8165	Na-8195
SCH J04374507+24043707	18.0	16.1	14.6	12.24	11.53	11.28	1.73	1.11	0.87
SCH J04374892+23341428	–	19.4	17.2	14.59	13.98	13.67	2.30	1.33	0.77
SCH J04383805+20171185	18.4	16.5	15.0	12.80	12.12	11.83	1.81	1.16	0.89
SCH J04385768+21463160	17.6	16.0	14.5	12.34	11.76	11.47	1.89	1.19	0.86
SCH J04394466+23315824	18.2	16.6	14.3	12.47	11.88	11.53	1.92	1.22	0.79
SCH J04394606+23025115	18.3	16.5	14.9	12.65	11.95	11.67	1.70	1.13	0.88
SCH J04395425+24230090	–	19.7	17.7	15.08	14.28	13.88	1.81	1.13	0.82
SCH J04402568+20205742	19.5	17.7	15.9	13.54	12.92	12.61	1.99	1.21	0.84
SCH J04410309+24164674	19.6	17.4	15.8	13.42	12.63	12.26	1.36	1.01	0.90
SCH J04415604+24135000	–	19.2	17.4	14.76	14.00	13.65	1.66	1.11	0.86
SCH J04425645+24275227	–	19.6	17.9	15.14	14.29	13.82	1.53	1.07	0.85
SCH J04434744+20251637	–	18.9	16.8	13.97	13.32	13.01	2.59	1.47	0.74
SCH J04464506+24364027	19.8	18.0	15.9	13.07	12.49	12.13	2.42	1.54	0.79
SCH J04464799+22075523	20.6	18.8	16.9	14.23	13.60	13.27	2.30	1.39	0.76
SCH J04482247+20514344	20.6	18.7	16.3	13.30	12.68	12.27	2.68	1.67	0.78
SCH J04490551+22031618	19.2	17.5	15.8	13.36	12.76	12.50	2.03	1.23	0.84
SCH J04490646+21522093	17.4	15.9	14.3	12.21	11.59	11.35	1.87	1.17	0.83
SCH J04520656+21002458	19.7	17.9	16.1	13.78	13.09	12.81	1.86	1.17	0.86
SCH J04524307+23332126	18.9	17.2	15.2	13.20	12.61	12.34	1.91	1.17	0.81
SCH J04531153+22341775	17.4	15.6	14.1	11.78	11.16	10.88	1.98	1.22	0.80
SCH J04541393+20230789	–	19.0	17.0	14.55	14.07	13.63	2.16	1.33	0.78
SCH J04545348+20521016	19.6	17.8	15.9	13.48	12.90	12.56	2.21	1.32	0.81
SCH J04582402+22151391	–	19.7	17.7	14.81	14.21	13.86	2.41	1.55	0.83
SCH J05003897+24225824	19.1	17.4	15.5	13.08	12.54	12.17	2.15	1.32	0.78
SCH J05005117+21462825	–	19.5	17.4	14.76	14.11	13.78	2.30	1.41	0.76
SCH J05010346+21043879	17.9	16.4	15.0	12.83	12.16	11.88	1.61	1.11	0.88
SCH J05011746+22335209	–	17.8	16.2	13.76	13.01	12.72	1.79	1.19	0.87
SCH J05023772+21540495	19.2	17.4	15.6	13.16	12.53	12.20	2.01	1.23	0.87
SCH J05033707+20230742	–	19.3	17.3	14.72	14.00	13.54	2.08	1.29	0.86
SCH J05050345+21044447	16.5	15.0	13.7	11.77	11.20	10.91	1.59	1.08	0.87
SCH J05055623+24291071	18.0	16.4	14.8	12.52	11.87	11.59	1.92	1.21	0.86
SCH J05061752+20514348	17.3	15.7	14.2	12.59	12.01	11.73	1.78	1.13	0.83
SCH J05061752+20514348	17.3	15.7	14.2	12.59	12.01	11.73	1.74	1.12	0.82
SCH J05065480+20542499	16.9	15.4	13.9	11.85	11.24	10.99	1.86	1.19	0.87
SCH J05094454+21452199	–	18.5	16.7	14.29	13.64	13.23	1.86	1.17	0.86
SCH J05110235+23574031	–	16.2	14.6	12.60	11.95	11.69	1.83	1.16	0.82
SCH J05115260+22444103	16.9	15.4	14.0	12.10	11.47	11.26	1.71	1.13	0.89

Table 4.2 (cont'd)

ID[a]	g	r	i	J[c]	H[c]	K_S[c]	TiO-7140	TiO-8165	Na-8195
SCH J05162541+21040800	19.1	17.4	15.7	13.36	12.80	12.49	2.09	1.29	0.81
SCH J05202425+24163845	–	20.0	18.1	15.40	14.51	14.10	1.74	1.14	0.87
SCH J05204088+20314071	18.5	16.8	15.1	12.90	12.28	12.03	2.02	1.21	0.86
SCH J05212398+23572292	–	19.0	17.0	14.39	13.72	13.32	2.35	1.42	0.79
SCH J05222623+21545792	18.5	16.9	15.3	13.19	12.59	12.34	1.91	1.21	0.84
SCH J05232027+24230192	20.2	18.5	16.5	14.05	13.46	13.09	2.20	1.31	0.79
SCH J05240100+21045046	17.2	15.5	13.9	11.81	11.23	10.95	1.85	1.18	0.82
SCH J05244136+24263530	18.8	17.2	15.5	13.29	12.73	12.43	1.92	1.20	0.80
SCH J05251535+21023971	–	19.5	17.0	13.29	12.63	12.24	1.78	2.02	0.78
SCH J05255410+23254047	–	18.6	16.7	14.26	13.51	13.21	1.74	1.09	0.87
SCH J05260810+23333802	–	19.4	17.4	14.78	14.03	13.65	1.79	1.15	0.82
SCH J05265150+24274728	19.2	17.3	15.7	13.29	12.59	12.29	1.77	1.17	0.86
SCH J05270113+23530238	–	19.8	18.0	15.32	14.48	14.10	1.59	1.12	0.83
SCH J05270681+23374776	–	19.8	17.7	15.03	14.30	14.02	2.39	1.39	0.78
SCH J05302983+24370854	18.8	17.1	15.3	13.05	12.40	12.10	2.07	1.30	0.81
SCH J05311984+23060478	17.6	15.9	14.4	12.21	11.65	11.41	1.85	1.19	0.83
SCH J05320030+21515747	16.8	15.3	13.7	11.50	10.87	10.56	1.97	1.21	0.79
SCH J05321214+20264183	17.6	15.9	14.2	11.85	11.23	10.93	2.08	1.28	0.79
SCH J05334071+20560298	18.1	16.6	15.0	12.88	12.25	12.01	1.87	1.19	0.83
SCH J05335346+23045373	19.4	17.7	15.9	13.51	12.93	12.64	2.05	1.25	0.84
SCH J05343049+20502794	16.1	14.7	13.5	11.88	11.26	11.04	1.48	1.05	0.87
SCH J05375244+23264770	15.9	14.4	12.9	11.00	10.41	10.17	1.65	1.09	0.83
SCH J05393117+23054477	19.3	17.3	15.6	13.27	12.65	12.34	2.07	1.25	0.78
SCH J05400118+20250873	18.9	17.2	15.3	12.94	12.36	12.04	2.14	1.30	0.79
SCH J05403786+24281777	–	18.9	16.9	14.17	13.49	13.15	2.38	1.46	0.80
SCH J05403868+21423466	19.1	17.3	15.6	13.44	12.94	12.61	2.01	1.23	0.84
SCH J05422003+22134842	15.6	14.1	12.9	11.14	10.51	10.25	1.49	1.10	0.90
SCH J05430011+22335091	–	19.3	17.4	14.69	14.03	13.72	2.34	1.47	0.84
SCH J05433937+23330204	18.6	16.8	14.4	12.14	11.50	11.19	2.27	1.36	0.78
SCH J05442656+22035440	18.5	16.9	15.3	13.11	12.48	12.18	1.90	1.17	0.85
SCH J05444476+20555487	18.7	16.8	15.1	12.85	12.22	11.94	2.01	1.25	0.78
SCH J05471468+23274615	–	19.8	17.3	14.18	13.46	13.16	2.57	1.69	0.77
SCH J05503959+24364706	19.2	17.5	15.8	13.57	12.99	12.69	2.11	1.28	0.85
SCH J05520649+21365149	18.9	17.2	15.8	13.89	13.30	13.05	1.64	1.11	0.85
SCH J05522087+20372913	19.9	18.0	16.1	13.74	13.15	12.86	2.06	1.27	0.87
SCH J05585296+21362200	20.2	18.4	16.8	14.71	14.15	13.78	1.74	1.31	0.87
SCH J05590744+23263037	18.6	17.1	15.5	13.50	12.86	12.58	1.69	1.12	0.88

Table 4.2 (cont'd)

ID[a]	g	r	i	J[c]	H[c]	K_S[c]	TiO-7140	TiO-8165	Na-8195

[a]Object IDs given in J2000 coordinates.

[b]Two faint candidates observed during the first spectroscopic observing run before the final photometric calibrations were finished do not have *r*-band photometry.

[c]Near-infrared photometry taken from 2MASS.